that we see in PSR B1931+24 may ultimately also help us to understand ordinary nulling. Whatever the cause is, it is conceivable that the onset of pulsar emission may be a violent event that may be revealed by high-energy observations. Although an archival search for x-ray or γ-ray counterparts for PSR B1931+24 has not been successful, the relatively large distance from the pulsar (~4.6 kpc) and arbitrary viewing periods may make such a detection unlikely.

The relation between the presence of pulsar emission via radiating particles and the increased spin-down rate of the neutron star provides strong evidence that a pulsar wind plays a substantial role in the pulsar braking mechanism. Although this has been suggested in the past (*12*), direct observational evidence has been missing so far. As a consequence of the wind's contribution to the pulsar spin-down, magnetic fields estimated for normal pulsars from their observed spin-down rates are likely to be overestimated.

The discovery of PSR B1931+24's behavior suggests that many more such objects exist in the Galaxy but have been overlooked so far because they were not active during either the search or confirmation observations. The periodic transient source serendipitously found recently in the direction of the galactic center (*13*) may turn out to be a short–time-scale version of PSR B1931+24 and hence to be a radio pulsar. In general, the time scales involved in the observed activity patterns of these sources pose challenges for observations scheduled with current telescopes. Instead, future telescopes with multibeaming capabilities, like the Square-Kilometre-Array or the Low Frequency Array, which will provide continuous monitoring of such sources, are needed to probe such time scales, which are still almost completely unexplored in most areas of astronomy.

References and Notes

1. A. G. Lyne, R. N. Manchester, J. H. Taylor, *Mon. Not. R. Astron. Soc.* **213**, 613 (1985).
2. G. H. Stokes, J. H. Taylor, J. M. Weisberg, R. J. Dewey, *Nature* **317**, 787 (1985).
3. G. Hobbs, A. G. Lyne, M. Kramer, C. E. Martin, C. Jordan, *Mon. Not. R. Astron. Soc.* **353**, 1311 (2004).
4. D. C. Backer, *Nature* **228**, 42 (1970).
5. I. H. Stairs, A. G. Lyne, S. Shemar, *Nature* **406**, 484 (2000).
6. F. C. Michel, *Theory of Neutron Star Magnetospheres* (Univ. of Chicago Press, Chicago, 1991).
7. F. Pacini, *Nature* **216**, 567 (1967).
8. J. E. Gunn, J. P. Ostriker, *Nature* **221**, 454 (1969).
9. A. K. Harding, I. Contopoulos, D. Kazanas, *Astrophys. J.* **525**, L125 (1999).
10. D. R. Lorimer, M. Kramer, *Handbook of Pulsar Astronomy* (Cambridge Univ. Press, Cambridge, 2005).
11. P. Goldreich, W. H. Julian, *Astrophys. J.* **157**, 869 (1969).
12. A. Spitkovsky, in *Young Neutron Stars and Their Environments, IAU Symposium 218*, F. Camilo, B. M. Gaensler, Eds. (Astronomical Society of the Pacific, San Francisco, CA, 2004), pp. 357–364.
13. S. D. Hyman *et al.*, *Nature* **434**, 50 (2005).
14. J. M. Cordes, T. J. W. Lazio, *NE2001. I. A New Model for the Galactic Distribution of Free Electrons and Its Fluctuations* (2002). Available at http://xxx.lanl.gov/abs/astro-ph/0207156.

15. D.R.L. is a University Research Fellow funded by the Royal Society.

19 December 2005; accepted 13 February 2006
Published online 23 February 2006;
10.1126/science.1124060
Include this information when citing this paper.

Quantum-Dot Spin-State Preparation with Near-Unity Fidelity

Mete Atatüre,[1]* Jan Dreiser,[1] Antonio Badolato,[1] Alexander Högele,[1,2] Khaled Karrai,[2] Atac Imamoglu[1]*

We have demonstrated laser cooling of a single electron spin trapped in a semiconductor quantum dot. Optical coupling of electronic spin states was achieved using resonant excitation of the charged quantum dot (trion) transitions along with the heavy-light hole mixing, which leads to weak yet finite rates for spin-flip Raman scattering. With this mechanism, the electron spin can be cooled from 4.2 to 0.020 kelvin, as confirmed by the strength of the induced Pauli blockade of the trion absorption. Within the framework of quantum information processing, this corresponds to a spin-state preparation with a fidelity exceeding 99.8%.

Semiconductor quantum dots (QDs) have been referred to as artificial atoms because of their discrete atom-like states. Photoluminescence (PL) studies of single QDs under nonresonant excitation have led to the generation of single photons (*1*, *2*) and cavity-quantum electrodynamics in the weak-coupling (*2*–*4*) and strong-coupling (*5*–*7*) regimes: all indicators of a quantum optical system. Similarly, resonant excitation has enabled the observation of Rabi oscillations (*8*) and coherent manipulation of excitons (*9*). These advances, in turn, have strengthened various proposals, including those regarding optical accessing of spins in QDs (*10*). However, from the perspective of quantum information processing (*11*), the ability to prepare, manipulate, and detect a spin qubit optically in solid-state systems is yet to be demonstrated.

We have demonstrated the high-fidelity preparation of a QD spin state via laser cooling [optical pumping (*12*)]. Using the Pauli blockade strength of the corresponding optical transitions as a means to infer the electron spin state, we showed that spin cooling due to spontaneous spin-flip Raman scattering can dominate over the heating introduced by hyperfine-induced spin-flip or cotunneling events. This allowed us to cool the spin temperature of an electron from 4.2 K (determined by the heat bath) down to 20 mK. By controlling the relative strength of these processes via gate voltage and magnetic field, we can tune the system from the regime of an isolated artificial atom to that of a quantum-confined solid-state system coupled either to a charge or a spin reservoir.

The experiments were performed on molecular-beam-epitaxy–grown single self-assembled InAs/GaAs QDs in a gated heterostructure, where the only difference as compared to the one used in (*13*) was the 35-nm tunnel barrier between the QD layer and the electron reservoir. In similar devices, a gate voltage applied between the ohmic and the Schottky contacts provides deterministic charging of QDs with signatures in the optical transitions (*14*). We performed the initial characterization of our QDs by conventional micrometer-resolution photoluminescence (μ-PL) spectroscopy at 4.2 K to determine the voltage range for each charging state, along with the associated optical transition frequencies. Figure 1A shows a typical gate sweep for our device, and the labels X^0 and X^{1-} identify the relevant optical transitions for our experiments: those from an empty QD and those from a single-electron–charged QD. We then carried out magneto-optical spectroscopy of the X^{1-} transition to extract the excitonic Zeeman splitting of 30 GHz/T. Having characterized the basic optical properties of the QD, we switched to resonant excitation using differential transmission technique: Fig. 1B shows a typical absorption plot at 0 T as a single-frequency laser is tuned across the trion transition. The details of this technique (*15*) along with its advantages in spin-selective measurements (*16*) can be found in previous works.

A single-electron–charged QD in the trion picture is analogous to the four-level system illustrated in Fig. 2A, where state $|\uparrow\downarrow, \blacktriangledown\rangle$ ($|\uparrow\downarrow, \blacktriangle\rangle$) corresponds to the QD with two ground-state electrons forming a singlet and a ground-state hole with angular momentum projection $J_z = -3/2$ (3/2) along the growth direction. The strong trion transitions, $|\uparrow\downarrow, \blacktriangledown\rangle \leftrightarrow |\downarrow\rangle$ and $|\uparrow\downarrow, \blacktriangle\rangle \leftrightarrow |\uparrow\rangle$, leave the resident electron spin unaltered, whereas the weak transitions, $|\uparrow\downarrow, \blacktriangledown\rangle \leftrightarrow |\uparrow\rangle$ and $|\uparrow\downarrow, \blacktriangle\rangle \leftrightarrow |\downarrow\rangle$, lead to a net spin-flip of the resident electron. The latter transitions are ideally forbidden by the optical selection rules; nevertheless, inherent heavy-light hole mixing

[1]Institute of Quantum Electronics, ETH Zurich, CH-8093 Zurich, Switzerland. [2]Center for NanoScience and Sektion Physik, Ludwig-Maximilians-Universität, 80539 Munich, Germany.

*To whom correspondence should be addressed. E-mail: atature@phys.ethz.ch (M.A.); imamoglu@phys.ethz.ch (A.I.)

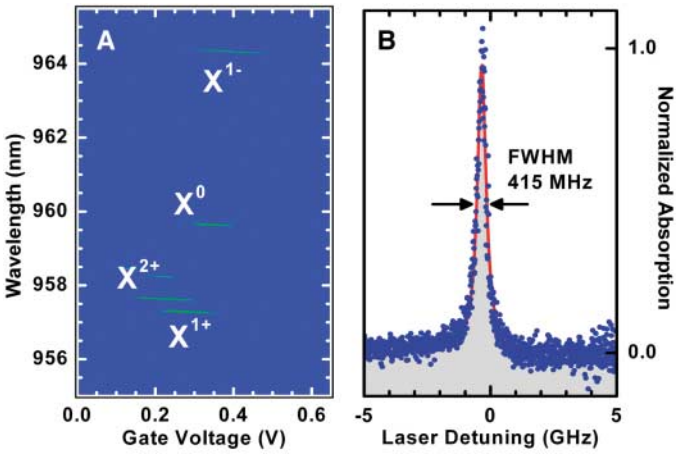

Fig. 1. (**A**) Photoluminescence from a single QD as a function of gate voltage. Each discrete jump in the emission spectrum corresponds to a charging state. Along with X^0 and $X^{1+(-)}$ lines, we observed a possible X^{2+} line, which corresponds to optically charged double resident holes. (**B**) Absorption peak of a single-electron–charged QD at a fixed gate voltage. The probe laser power was 10 nW, corresponding to a Rabi frequency $\Omega_L = 0.25\ \Gamma$, and the absolute value of absorption was 0.4%. The full width at half maximum (FWHM) of the transition was 415 MHz.

or a magnetic field that is not parallel to the strong confinement (z) axis yields $\Gamma \gg \gamma \neq 0$, where Γ and γ are the allowed and forbidden spontaneous emission rates, respectively, as indicated in Fig. 2A. In addition to these optical transitions, the strong hyperfine interaction of the resident electron spin with the QD nuclear spin ensemble leads to random spin-flip events at rate $\xi_{\uparrow\downarrow}$. Previous studies on similar structures have shown that $\xi_{\uparrow\downarrow}^{(B\,=\,0)} \leq \Gamma$ in the absence of an external magnetic field B but is strongly suppressed even under relatively weak magnetic fields ($B \sim 0.1$ T) because of incommensurate electron and nuclear Zeeman energies (*17*, *18*). This is the case depicted in Fig. 2B, where $\xi_{\uparrow\downarrow}^{(B\,>\,0)} \ll \gamma$. When a second re-pump laser is resonant with the other Zeeman-split trion transition $|\uparrow\downarrow, \blacktriangle\rangle$ — $|\uparrow\rangle$ (Fig. 2C), the $|\uparrow\rangle \rightarrow |\downarrow\rangle$ transition will also take place via spontaneous spin-flip Raman scattering, with a rate proportional to the laser intensity.

Figure 2D is the absorption analog of Fig. 1A, showing the expected X^{1-} plateau at $B = 0$ T, where the QD is single-electron-charged for gate voltages (V_{gate}) in the 320- to 424-mV range. The probe laser was scanned across the $|\uparrow\downarrow, \blacktriangledown\rangle$ — $|\downarrow\rangle$ transition and had the corresponding circular polarization [$\sigma^{(-)}$] as determined by the optical selection rules. Figure 2E shows a suppression of the X^{1-} plateau at a 0.2-T magnetic field: The QD becomes transparent for gate voltages in the 344- to 396-mV range. Given that the corresponding X^0 plateau remains unaffected under all magnetic fields, this strong suppression of the signal in the X^{1-} plateau center is a signature of optical electron-spin pumping into the $|\uparrow\rangle$ state due to the unidirectional spontaneous Raman scattering process (γ) that dominates over the bidirectional spin-flip process ($\xi_{\uparrow\downarrow}^{(B\,>\,0)}$). In this case, we can confirm that the electron remained in the spin-up state 98.5% of the time, as the laser was resonant with the Pauli-blocked (*16*, *19*) $|\uparrow\downarrow, \blacktriangledown\rangle$ — $|\downarrow\rangle$ transition of the electronic spin-down state. A similar measurement at 0.3 T showed that the electron was in the $|\uparrow\rangle$ state 99.8% of the measurement time. To date, this value is the highest state-preparation fidelity reported in a solid-state system (*20*, *21*) and was achieved for both electron-spin states. The verification of higher-fidelity values is not limited by the physical mechanism involved but rather by our signal-to-noise level (*22*).

To prove that the electron was shelved in the $|\uparrow\rangle$ state by the probe laser at the $|\uparrow\downarrow, \blacktriangledown\rangle$ — $|\downarrow\rangle$ transition, we simultaneously applied a re-pump laser on the $|\uparrow\downarrow, \blacktriangle\rangle$ — $|\uparrow\rangle$ transition with orthogonal circular polarization [$\sigma^{(+)}$]. Figure 2F shows the resulting gate sweep, where an absorption peak at $V_{gate} = 372$ mV appears. The linewidth of this peak is equal to that shown in Fig. 1B, and it was observed when the re-pump laser was detuned from the probe laser by exactly 6 GHz; that is, the independently measured Zeeman splitting of the X^{1-} transition. The fact that we recovered the probe laser absorption only when both lasers were resonant with the corresponding trion transitions indicates that the re-pump laser allowed for bidirectional spin-flip spontaneous Raman scattering and prohibited any net spin shelving: The system is now described by the illustration in Fig. 2C. When we kept the frequency of the re-pump laser unchanged but increased the magnetic field to 0.3 T, we observed that the absorption peak on the transparent section of the plateau shifted in accordance with the corresponding 9-GHz Zeeman splitting.

Figure 3A shows the magnetic-field dependence of the absorption displaying the Pauli blockade strength in the middle of the charging plateau, normalized to the maximum absorption at 0 T. Because Γ and γ have no magnetic-field dependence, our measurements reveal the magnetic-field dependence of the hyperfine-induced spin-flip rate $\xi_{\uparrow\downarrow}^{(B\,>\,0)}$. The red line is a theoretical curve obtained from rate equations by taking into account both photon-assisted hyperfine-induced spin-flip events and the spontaneous spin-flip Raman transition. The parameters used to simulate the experimental results are $\Gamma = 300$ MHz; $\gamma = 100$ kHz; the effective Overhauser field arising from randomly oriented nuclear spins (B_{nuc}) = $A/\sqrt{N} = 12.5$ mT (*23*); and the electronic g factor (g_e) = –0.6 (*24*). The spin cooling rate (below saturation) is independent of laser power for the single-Λ system, further supporting our assumption that both cooling and spin relaxation are (linearly) proportional to the intensity of the probe laser. We emphasize, however, that an exponential fit seems to be in better agreement with the data, indicating that our simple theoretical model may not be capturing other relevant processes such as phonon-assisted spin-flips or spin-orbit coupling.

The triangles at 0.2 T in Fig. 3A correspond to the partial (full) recovery of the absorption as the bidirectional optical spin pumping was realized using the re-pump laser, which was of weaker (comparable) intensity with respect to the probe laser. The state-preparation fidelity for the electron spin as a function of magnetic field is plotted in Fig. 3B. At 0.3 T, the electron is already in the spin-up state, with a fidelity exceeding 99.8%. With each data point, the corresponding spin temperature is provided as obtained from the state occupancies, and a net cooling from 4.2 to 20 mK is achieved. As a token of our cooling efficiency, we emphasize that such state-preparation fidelity can be achieved only at a 62-T external field, when one relies solely on thermal equilibration at 4.2 K in the absence of laser cooling.

Another striking feature of the gate sweep depicted in Fig. 2E is that the absorption remains essentially unaffected for gate voltages that define the edges of the plateau. Spin cooling is ineffective in this regime despite the fact that the hyperfine-induced electron spin-flip rate should not depend on the gate voltage. On the other hand, it has been shown that the cotunneling-induced spin-flip rate varies across the absorption plateau by a factor as large as 10^6 (*25*) for 20-meV electron charging energy (*26*). We expect the electron spin-flip rate $\xi_{\uparrow\downarrow}^{(B)}$ to be dominated by cotunneling at the edges of the plateau, leading to a suppression of spin pumping. In more general terms, the spin-cooling dynamics is determined by interplay between spontaneous spin-flip Raman scattering, hyperfine-induced electron spin-flips, and electronic cotunneling processes. In the absence of magnetic field and at a gate voltage within the plateau middle, QD spin strongly interacts with the QD nuclei. Alternatively, at finite magnetic field and at a gate voltage within the edges of the plateau, QD spin strongly interacts with the back-gate electron reservoir. In both regimes, the electron spin cannot be considered as an isolated quantum system any more because of its dominant coupling to a spin or a charge reservoir.

The next step after gaining a full understanding of and control over such spin dynamics will be to

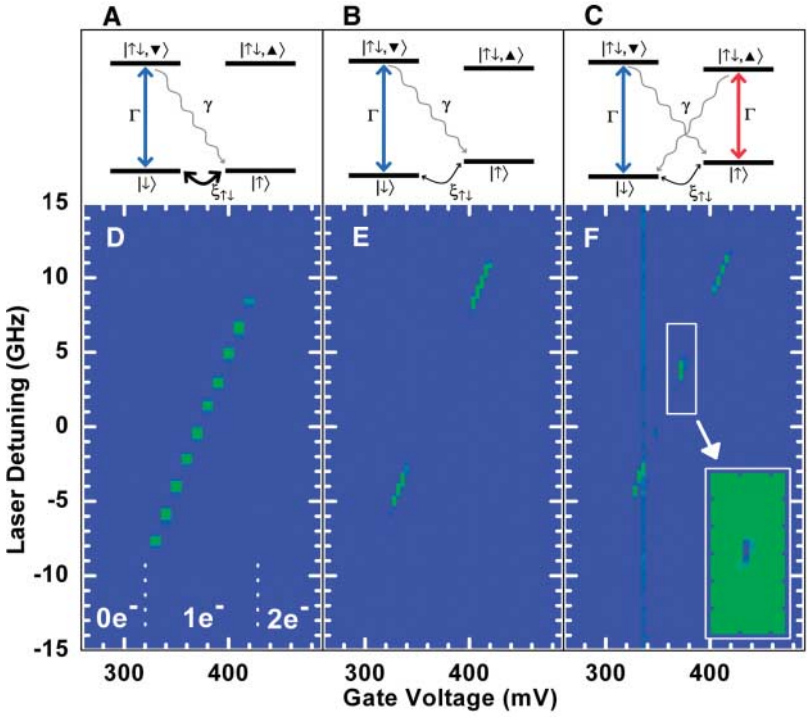

Fig. 2. (**A**) Four-level scheme illustrating the ground and excited states of a single-electron–charged QD. Because $\xi_{\uparrow\downarrow}^{(B=0)}$ is relatively strong when the spin states are degenerate, the optical transitions do not alter spin-state occupancies. (**B**) When the degeneracy is lifted by a magnetic field, the optical transitions form a Λ system, which in turn allows for spin cooling via spin-flip spontaneous Raman transition under the condition $\Gamma \gg \gamma \gg \xi_{\uparrow\downarrow}$. (**C**) A symmetric double-Λ system allows for bidirectional spin pumping, and therefore manipulation of spin-state occupancies can be achieved as a function of laser intensity ratios. (**D**) Absorption as a function of probe-laser frequency and 10-mV gate voltage increments in the absence of a magnetic field. The slope is determined by the DC-Stark shift. Absorption is constant throughout the voltage plateau, which identifies the range for single-electron charging of the QD. (**E**) Same plateau with finer (4-mV) gate voltage increments under a 0.2-T magnetic field. The plateau middle is suppressed as spin cooling takes effect and induces strong Pauli blockade on the investigated transition. Indeed, we nearly achieved 10^3-fold suppression. The remaining absorption at the plateau edges coincides with the strong cotunneling regime. The spectral displacement of the plateau is due to the diamagnetic and Zeeman shifts, as imprinted in the 4-GHz detuning from the probe laser. (**F**) Same plateau in the presence of a re-pump laser detuned by 6 GHz with respect to the probe laser. Ultra–high-fidelity spin cooling is still observed, except when both lasers are simultaneously resonant with the 6-GHz-split Zeeman transitions. At this point, the double-Λ system of (C) is realized, and the sharp resonance peak within the suppressed part of the plateau is the confirmation for this realization. (Inset) A finer scan of the indicated rectangle; each tick on the *y* axis corresponds to 1 GHz.

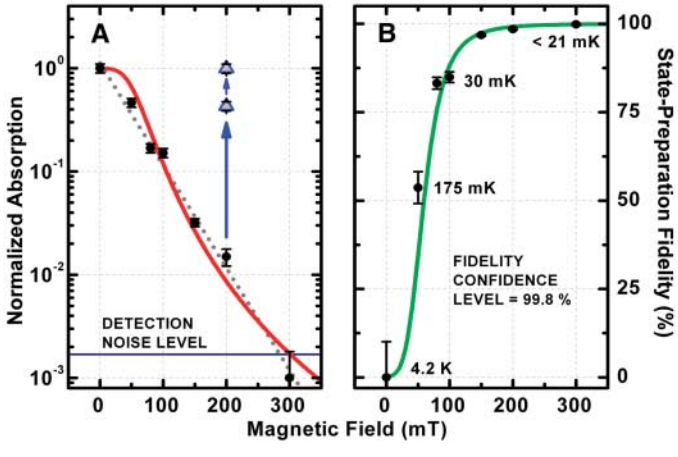

Fig. 3. (**A**) Magnetic field dependence of the absorption at V_{gate} = 372 mV. A nearly 10^3-fold suppression is obtained because of Pauli blockade in the single-Λ scheme. In the double-Λ scheme, absorption depends on the intensity ratio of the two lasers. The triangles indicate the partial (full) recovery of the absorption signal when $P_{re\text{-}pump} = 0.25\ P_{probe}$ ($P_{re\text{-}pump} = P_{probe}$). (**B**) State-preparation fidelity with increasing magnetic field. At 0.3 T, the electron is already prepared in the spin-up state with at least 99.8% fidelity. The electron-spin temperature is provided for each data point.

tune the spin-flip Raman transition rate as a function of magnetic field orientation with respect to the strong confinement axis. Our results constitute the first step toward stimulated Raman transition (*27*) on a single QD electron for coherent preparation of an arbitrary superposition of spin states, as well as cavity-assisted spin-flip Raman transitions as a source of indistinguishable single photons with near-unity collection efficiency (*28*). The electron-spin cooling mechanism described here can alternatively be used for dynamical nuclear-spin polarization.

References and Notes

1. P. Michler *et al.*, *Science* **290**, 2282 (2000).
2. C. Santori, D. Fattal, J. Vučković, G. S. Solomon, Y. Yamamoto, *Nature* **419**, 594 (2002).
3. A. Kiraz *et al.*, *Appl. Phys. Lett.* **78**, 3932 (2001).
4. T. D. Happ *et al.*, *Phys. Rev. B* **66**, R041303 (2002).
5. J. P. Reithmaier *et al.*, *Nature* **432**, 197 (2004).
6. T. Yoshie *et al.*, *Nature* **432**, 200 (2004).
7. E. Peter *et al.*, *Phys. Rev. Lett.* **95**, 067401 (2005).
8. A. Zrenner *et al.*, *Nature* **418**, 612 (2002).
9. X. Li *et al.*, *Science* **301**, 809 (2003).
10. A. Imamoğlu *et al.*, *Phys. Rev. Lett.* **83**, 4204 (1999).
11. D. P. DiVincenzo, *Fortschr. Phys.* **48**, 771 (2000).
12. J. Brossel, A. Kastler, J. Winter, *J. Phys. Radium* **13**, 668 (1952).
13. H. Drexler, D. Leonard, W. Hansen, J. P. Kotthaus, P. M. Petroff, *Phys. Rev. Lett.* **73**, 2252 (1994).
14. R. J. Warburton *et al.*, *Nature* **405**, 926 (2000).
15. B. Alén, F. Bickel, K. Karrai, R. J. Warburton, P. M. Petroff, *Appl. Phys. Lett.* **83**, 2235 (2003).
16. A. Högele *et al.*, *Appl. Phys. Lett.* **86**, 221905 (2005).
17. J. M. Elzerman *et al.*, *Nature* **430**, 431 (2004).
18. M. Kroutvar *et al.*, *Nature* **432**, 81 (2004).
19. T. Calarco, A. Datta, P. Fedichev, E. Pazy, P. Zoller, *Phys. Rev. A.* **68**, 012310 (2003).
20. J. R. Petta *et al.*, *Science* **309**, 2180 (2005).
21. R. Hanson *et al.*, *Phys. Rev. Lett.* **94**, 196802 (2005).
22. All of these measurements were performed on time scales faster than significant dynamical nuclear-spin polarization (*29*, *30*) so as to avoid any alteration of the trionic absorption spectrum. This time scale of ~300 ms, which corresponds to how long the laser remains resonant with the transition, in turn defined our detection-noise level.
23. A. C. Johnson *et al.*, *Nature* **435**, 925 (2005).
24. Γ = 300 MHz and $g_e = -0.6$ are average values measured on numerous QDs within this sample. B_{nuc} = 12.5 mT implies 10^5 nuclei within the QD, which in turn is consistent with transmission electron microscope images of similar QDs. The X^0 and X^{1-} transition linewidths give an upper bound of 20 mT for B_{nuc}.
25. J. M. Smith *et al.*, *Phys. Rev. Lett.* **94**, 197402 (2005).
26. The absorption linewidth at the edge of the plateau is not broader than that at the center, suggesting a tunneling rate less than 300 MHz, which puts an upper limit of 0.3 KHz on the cotunneling rate. Further, the absorption peak in the plateau center does not saturate above our detection-noise level (Fig. 3A), indicating that the cotunneling rate must be at least 10^3 slower than γ. This, in turn, marks a more accurate upper bound of 0.1 KHz.
27. M. V. G. Dutt *et al.*, *Phys. Rev. Lett.* **94**, 227403 (2005).
28. A. Kiraz, M. Atatüre, A. Imamoğlu, *Phys. Rev. A* **69**, 032305 (2004).
29. S. W. Brown, T. A. Kennedy, D. Gammon, E. S. Snow, *Phys. Rev. B* **54**, R17339 (1996).
30. C. W. Lai, P. Maletinsky, A. Badolato, A. Imamoğlu, *Phys. Rev. Lett.*, in press.

31. Supported by the National Centers of Competence in Research Quantum Photonics. M.A. and J.D. thank J. Cash for technical assistance.

10 February 2006; accepted 28 March 2006
Published online 6 April 2006;
10.1126/science.1126074
Include this information when citing this paper.